

Optimal Transport-Guided Safety in Temporal Difference Reinforcement Learning

Zahra Shahrooei and Ali Baheri

Abstract—The primary goal of reinforcement learning is to develop decision-making policies that prioritize optimal performance, frequently without considering safety. In contrast, safe reinforcement learning seeks to reduce or avoid unsafe behavior. This paper views safety as taking actions with more predictable consequences under environment stochasticity and introduces a temporal difference algorithm that uses optimal transport theory to quantify the uncertainty associated with actions. By integrating this uncertainty score into the decision-making objective, the agent is encouraged to favor actions with more predictable outcomes. We theoretically prove that our algorithm leads to a reduction in the probability of visiting unsafe states. We evaluate the proposed algorithm on several case studies in the presence of various forms of environment uncertainty. The results demonstrate that our method not only provides safer behavior but also maintains the performance. A Python implementation of our algorithm is available at <https://github.com/SAILRIT/OT-guided-TD-Learning>.

I. INTRODUCTION

Safe reinforcement learning (RL) algorithms are essential for many real-world applications in robotics [1], autonomous systems [2], finance [3], and healthcare [4]. Various approaches have been explored to integrate safety into RL. A comprehensive review of these methods can be found in [5].

Several early safe RL studies incorporate safety into the optimization criterion [6]–[11]. For example, in the worst-case criterion, a policy is considered optimal if it maximizes the worst-case return, which reduces variability due to inherent or parameter uncertainty [6], [7]. The optimization criterion can also be adjusted to balance return and a risk metric, such as a linear combination of return and the variance of return [8] or as the probability of entering an error state [9]. The other way is to optimize the return subject to constraints, resulting in the constrained optimization criterion [10]–[12]. Other approaches aim to avoid heuristic exploration strategies, which are blind to the safety of actions. Instead, they propose modifications to the exploration process to guide the agent toward safer regions. Safe exploration techniques include prior knowledge of the task for search initialization [13], learn from human demonstrations [14], and incorporate a risk metric into the algorithm [15], [16].

In the latter, uncertainty estimates are commonly used to direct exploration and enhance policy stability. To accomplish this, a method is to estimate the uncertainty of future returns. For example, O’Donoghue *et al.* [17] propose an uncertainty Bellman equation to approximate the variance of Q-value posterior distributions. Distributional RL studies

[18]–[22] explicitly estimate the distribution of returns and measure aleatory uncertainty, which originates from intrinsic stochasticity in the environment and is irreducible. Our work differs from these works in that we do not need the return distribution to guide the agent toward taking safer actions. There are other works that use information-directed sampling to prevent the negative consequences of aleatory uncertainty by making a trade-off between instantaneous regret and information gain [23], [24]. However, these information-directed approaches require learning the transition dynamics of the environment. An alternative approach is to assess the uncertainty in the model dynamics rather than concentrating on the uncertainty of the returns. For instance, Yu *et al.* [25] estimate the uncertainty of the dynamics model and penalize actions that result in uncertain returns. Our method differs from these approaches because it does not require any model or prior knowledge of the dynamics to direct the exploration.

In this work, we define safety in stochastic environments as choosing actions with more predictable consequences. We explore the use of optimal transport (OT) theory to quantify the uncertainty level corresponding to different actions. OT is highly valued for its ability to measure and optimize the alignment between probability distributions [26] by minimizing the cost of transforming one distribution into another while taking into account the geometry of the distributions as shown in Fig. 1. There are a few applications of OT in safe RL [27]–[33]. For example, Metelli *et al.* [30] propose a novel approach called Wasserstein Q-learning (WQL), which uses Bayesian posterior distributions and Wasserstein barycenters to model and propagate uncertainty in RL. Their method demonstrates improved exploration and faster learning in tabular domains compared to classic RL algorithms. Baheri [27] uses OT for reward shaping in Q-learning. Through the minimization of the Wasserstein distance between the policy’s stationary distribution and a predefined safety distribution over state space, the agent is encouraged to visit safe states more frequently.

In this paper, we propose an OT-based temporal difference (TD) framework that considers both the reward and the uncertainty associated with actions without relying on expert knowledge or predefined safety constraints. We use Wasserstein distance to quantify the total uncertainty score at each state and prioritize the actions that contribute less to this score. This encourages the agent to take less uncertain actions more frequently, which leads to safer overall behavior.

The contributions of this paper are: (i) introduction of an OT-guided TD learning algorithm to enhance agent safety

Zahra Shahrooei and Ali Baheri are with the Department of Mechanical Engineering, Rochester Institute of Technology, Rochester, NY 14623 USA. (e-mail: zs9580@rit.edu; akbeme@rit.edu).

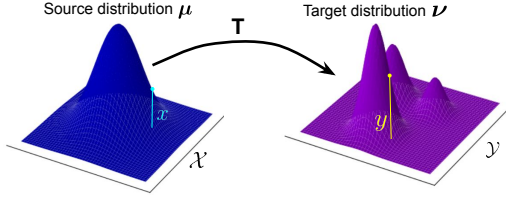


Fig. 1: Conceptual illustration of optimal transport theory. Here, $\mu(x)$ is a probability distribution over the source space \mathcal{X} , and $\nu(y)$ is a probability distribution over the target space \mathcal{Y} . The arrows represent the optimal transport plan T , which reallocates mass from μ to ν to minimize the total transport cost $c(x, y)$.

by integrating action uncertainty into decision-making in addition to the reward signal without requiring prior expert knowledge or safety constraints, (ii) deriving safety bounds of the algorithm which demonstrates less visitation to unsafe states (Theorem 1), and (iii) applications on various case studies under different forms of uncertainty in reward function, transition function, and states to show our algorithm reduces visiting unsafe states while preserving performance.

We structure this paper as follows: Section II provides a mathematical overview of temporal difference learning and optimal transport theory. Section III elaborates on incorporating optimal transport-based action uncertainty into temporal difference learning. Section IV presents experiments on various environments and their results. Section V concludes and suggests future direction.

II. PRELIMINARIES

This section reviews Markov decision processes, partially observable Markov decision processes, temporal difference learning algorithms, and the basic principles of OT theory.

A. MARKOV DECISION PROCESSES AND TEMPORAL DIFFERENCE LEARNING

Markov Decision Processes (MDPs). MDPs [34] represent a fully observable RL environment. A finite MDP is defined by the tuple $\mathcal{M} = (\mathcal{S}, \mathcal{A}, \mathcal{T}, \mathcal{R}, \gamma)$, where \mathcal{S} is a set of states, \mathcal{A} is a set of actions, $\mathcal{T} : \mathcal{S} \times \mathcal{A} \times \mathcal{S} \rightarrow [0, 1]$ is the transition probability function, where $\mathcal{T}(s'|s, a)$ represents the probability of transitioning to state s' when action a is taken in state s , $\mathcal{R} : \mathcal{S} \times \mathcal{A} \rightarrow \mathbb{R}$ is the reward function where $\mathcal{R}(s, a) = r$ represents the immediate reward received for taking action a in state s , and $\gamma \in [0, 1]$ is the discount factor. The agent follows a policy $\pi : \mathcal{S} \times \mathcal{A} \rightarrow [0, 1]$ that maps states to action probabilities, with the objective to maximize the expected discounted return, $G_t = \sum_{k=0}^{\infty} \gamma^k r_{t+k+1}$.

Temporal Difference Learning. The Q-value of action a in state s under policy π is given by $Q_{\pi}(s, a) = \mathbb{E}_{\pi}[G_t | s_t = s, a_t = a]$, which can be incrementally learned. In one-step TD, the Q-value update rule is $Q(s_t, a_t) \leftarrow Q(s_t, a_t) + \alpha \delta_t$ where δ_t is the TD error at time t and α is the learning rate.

In Q-learning algorithm [35], the TD error is defined as:

$$\delta_t = r_{t+1} + \gamma \max_a Q(s_{t+1}, a) - Q(s_t, a_t) \quad (1)$$

Similarly, in SARSA algorithm [34], the TD error is given by:

$$\delta_t = r_{t+1} + \gamma Q(s_{t+1}, a_{t+1}) - Q(s_t, a_t). \quad (2)$$

SARSA(λ) extends one-step SARSA using eligibility traces to incorporate multi-step updates and improve learning efficiency [34]. An eligibility trace tracks the degree to which each state-action pair has been recently visited, which enables updates to consider a weighted history of past experiences. The Q-value update rule in SARSA(λ) is:

$$Q_{t+1}(s, a) = Q_t(s, a) + \alpha \delta_t e_t(s, a) \quad (3)$$

where $e_t(s, a)$ is the eligibility trace. The eligibility trace $e_t(s, a)$ decays over time and is updated as follows:

$$e_t(s, a) = \begin{cases} \gamma \lambda e_{t-1}(s, a) + 1 & \text{if } s = s_t \text{ and } a = a_t \\ \gamma \lambda e_{t-1}(s, a) & \text{otherwise} \end{cases} \quad (4)$$

where $\lambda \in [0, 1]$ controls the trace decay rate. TD algorithms often use an ϵ -greedy strategy for action generation. The parameter ϵ can either be fixed or decay over time to balance exploration and exploitation. The behavioral policy is expressed as:

$$\pi(s_t, a_t) = \begin{cases} 1 - \epsilon + \frac{\epsilon}{|\mathcal{A}|} & \text{if } a_t = \arg \max_{a'_t} Q(s_t, a'_t) \\ \frac{\epsilon}{|\mathcal{A}|} & \text{otherwise} \end{cases} \quad (5)$$

Partially Observable MDPs (POMDPs). POMDPs [36] generalize MDPs to account for environments where the agent cannot directly observe the underlying state. A POMDP is defined by the tuple $\mathcal{POMDP} = (\mathcal{S}, \mathcal{A}, \mathcal{O}, \mathcal{T}, \mathcal{R}, \mathcal{Z}, \gamma)$, where \mathcal{S} , \mathcal{A} , \mathcal{T} , \mathcal{R} , and γ maintain their definitions from MDPs, and \mathcal{O} is a set of observations the agent can perceive. The observation function $\mathcal{Z} : \mathcal{S} \times \mathcal{A} \rightarrow \mathcal{O}$ maps states and actions to observation probabilities.

B. OPTIMAL TRANSPORT THEORY

The OT theory aims to find minimal-cost transport plans to move one probability distribution to another within a metric space. This involves a cost function $c(x, y)$ and two probability distributions, $\mu(x)$ and $\nu(y)$. The goal is to find a transport plan that minimizes the cost of moving μ to ν under $c(x, y)$, often using the Euclidean distance for explicit solutions [37].

We focus on discrete OT theory, assuming μ and ν as source and target distributions, respectively, both belonging to $\mathcal{Pp}(\mathbb{R}^n)$, i.e., they are probability measures with finite p -th moments [37] with finite supports $\{x_i\}_{i=1}^{m_1}$ and $\{y_j\}_{j=1}^{m_2}$, and corresponding probability masses $\{a_i\}_{i=1}^{m_1}$ and $\{b_j\}_{j=1}^{m_2}$. The cost between support points is represented by an $m_1 \times m_2$ matrix C , where $C_{ij} = |x_i - y_j|_p^p$ denotes the transport cost from x_i to y_j . The OT problem seeks the transport plan P^* that minimizes the cost while ensuring that the marginals of P^* match μ and ν :

$$\min_{P \in \mathbb{R}^{m_1 \times m_2}} \sum_{i=1}^{m_1} \sum_{j=1}^{m_2} P_{ij} C_{ij} \quad (6)$$

Here, the coupling matrix P_{ij} indicates the probability mass transported from x_i to y_j and $\sum_{j=1}^{m_2} P_{ij} = a_i$ for all i , and $\sum_{i=1}^{m_1} P_{ij} = b_j$ for all j . Additionally, $P_{ij} \geq 0$ for all i, j .

Definition 1 [37]: The Wasserstein distance between μ and ν is computed using the OT plan P^* obtained from solving the above linear programming problem:

$$W_p(\mu, \nu) = (\langle P^*, C \rangle)^{\frac{1}{p}} \quad (7)$$

where $p \geq 1$ and $\langle \cdot, \cdot \rangle$ denotes the inner product.

To enhance numerical stability and computational efficiency, an entropy regularization term can be added to the objective, leading to the regularized Wasserstein distance, which can be solved iteratively using the Sinkhorn iterations [38].

Definition 2 [38]: The Entropy-regularized OT problem is formulated as:

$$\min_{P \in \mathbb{R}^{m_1 \times m_2}} \sum_{i=1}^{m_1} \sum_{j=1}^{m_2} P_{ij} C_{ij} + \varepsilon \sum_{i=1}^{m_1} \sum_{j=1}^{m_2} P_{ij} (\log P_{ij} - 1) \quad (8)$$

where $\varepsilon > 0$ is a regularization parameter that balances transport cost and the entropy of the transport plan P .

III. METHODOLOGY

Consider an RL agent interacting with an environment defined by a discrete MDP $\mathcal{M} = (\mathcal{S}, \mathcal{A}, \mathcal{T}, \mathcal{R}, \gamma)$, where a subset of states $\mathcal{S}_u \subset \mathcal{S}$, denoted as unsafe states, exhibits stochasticity in the reward function \mathcal{R} or transition function \mathcal{T} . These unsafe states are undesirable due to their unpredictable outcomes, and the agent aims to visit them less frequently to enhance safety. For each state s , we define the *Q-distribution* Q_s as the normalized distribution over the agent's estimated Q-values for the available actions a_i , $i = 1, \dots, N$. Formally, we have

$$Q_s = \sum_{i=1}^N q_i^s \delta_{a_i} \quad (9)$$

where q_i^s is the probability assigned to action a_i based on the current Q-value estimations, and δ_{a_i} is the Dirac measure centered at a_i . Intuitively, Q_s captures how the agent's Q-values are distributed across actions at state s . We also introduce a corresponding T-distribution T_t , which is constructed similarly to the Q-distribution but is derived from the target values used in SARSA update rule. Specifically, for each state s and each action a_i in s , we maintain a target value in a buffer, which is updated whenever a_i is selected in s . When the agent chooses action a_t in state s_t , the target value for (s_t, a_t) is updated to $r_{t+1} + \gamma Q(s_{t+1}, a_{t+1})$, where r_{t+1} is the observed reward and γ is the discount factor. For actions $a_i \neq a_t$ in state s_t , the target value preserves the value from the most recent instance in which a_i was selected in s_t . Hence, we have

$$T_t = \sum_{i=1}^N p_i^t \delta_{a_i} \quad (10)$$

where p_i^t is the probability associated with action a_i based on target values.

For each action a_i in state s , we define an uncertainty score $U(s, a_i)$. The goal is to quantify how much an action contributes to the overall uncertainty score of the agent's policy in that state. First, we compute the OT map P^* between Q_s and T_t by solving the entropy-regularized Wasserstein distance formulation. We note that here, the cost matrix $C(a_i, a_j)$, for $i, j = 1, \dots, N$ is inherently task-dependent and its definition varies depending on the structure of the action space. The total uncertainty score in state s is measured by the Wasserstein distance $W(Q_s, T_t)$. For an action a_i , the flow $\Delta(s, a_i)$ is defined as the absolute difference between the outgoing flow (transport from a_i to other actions $b \neq a_i$) and the incoming flow (transport from other actions $b \neq a_i$ to a_i):

$$\Delta(s, a_i) = \left| \sum_{b \neq a_i} P_{a_i, b}^* - \sum_{b \neq a_i} P_{b, a_i}^* \right| \quad (11)$$

Here, the first summation $\sum_{b \neq a_i} P_{a_i, b}^*$ represents how much probability mass is transported away from a_i to other actions, while the second summation $\sum_{b \neq a_i} P_{b, a_i}^*$ denotes how much mass flows into a_i from other actions. The absolute difference between these two flows, $\Delta(s, a_i)$, captures how much the probability of an action in Q_s must be “redistributed” to match T_t . We subsequently normalize this value by the total uncertainty in state s :

$$U(s, a_i) = \frac{\Delta(s, a_i)}{W(Q_s, T_t)} \quad (12)$$

The uncertainty score $U(s, a_i)$ thus reflects how much action a_i is responsible for the mismatch between Q_s and T_t . Equivalently, it reveals to what extent the action a_i needs to be adjusted for Q_s to align with T_t in a cost-efficient manner. Higher values of $\Delta(s, a_i)$ indicate larger corrections to the probability of a_i in Q_s , which suggests more unpredictable outcomes. While standard SARSA does not account for safety, we incorporate the above uncertainty score into the behavioral policy. Let β be a sensitivity coefficient that specifies how strongly the agent prioritizes safety relative

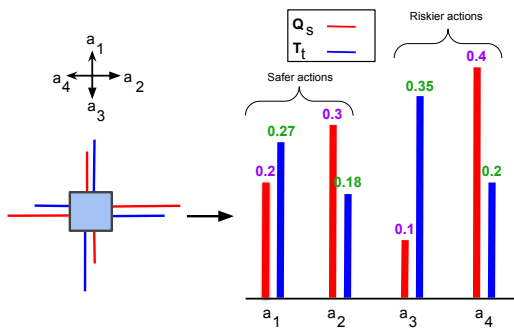


Fig. 2: Example: For a fixed state and four available actions, we compute the uncertainty score of the state $W(Q_s, T_t)$ and the contribution of each action to this uncertainty score.

to reward. We then modify the ϵ -greedy behavioral policy π^b as follows:

$$\pi^b(a | s) = \begin{cases} 1 - \epsilon + \frac{\epsilon}{|\mathcal{A}|} & \text{if } a = \arg \max_{a'} [Q(s, a') - \beta U(s, a')] \\ \frac{\epsilon}{|\mathcal{A}|} & \text{otherwise.} \end{cases} \quad (13)$$

where the ϵ component guarantees infinite exploration of all actions in visited states over time. Actions that lead to unsafe states typically have higher uncertainty scores $U(s, a)$ due to the stochasticity of those states, which increases the flow imbalance $\Delta(s, a)$. This property enables the algorithm to prioritize safer actions and reduce the likelihood of visiting \mathcal{S}_u . In other words, the agent's action-selection process is biased to favor actions with both high Q-values and low uncertainty scores. Indeed, we encourage the agent to choose the action for which it has the highest confidence in the outcome among the actions experienced in that state. This approach enables a directed exploration strategy that prioritizes safer actions with higher rewards. Example 1 further illustrates the influence of this uncertainty score on both Q-values and policy decisions. In particular, it demonstrates the trade-off between exploiting high-return actions and mitigating highly uncertain actions to ensure safer exploration and more stable learning.

In the context of POMDPs, we use SARSA(λ) variant. Specifically, Q_s and T_t distributions associated with the agent's current observation o and the available actions a_1, \dots, a_N are integrated into the uncertainty score term $U(o, a_i)$. Moreover, the flexibility of our approach enables its extension to scenarios that involve using multiple consecutive observations o_{t-n}, \dots, o_t , which can help the algorithm better capture non-Markovian properties.

Example: Consider a fixed state s with four available actions. For this state, we have access to Q_s and T_t distributions over actions as depicted in Fig. 2. Table I shows how the uncertainty score term affects the Q-values and action selection. As observed, a_1 is the safest action and a_4 offers the highest reward. In decision-making, standard SARSA prefers action a_4 , whereas OT-guided SARSA chooses a_2 to balance the reward and safety.

Theorem 1: Given a finite MDP $\mathcal{M} = (\mathcal{S}, \mathcal{A}, \mathcal{T}, \mathcal{R}, \gamma)$ with state space \mathcal{S} and action space \mathcal{A} , let $\mathcal{S}_u \subset \mathcal{S}$ be a set of unsafe states to avoid. We define π^0 as the ϵ -greedy

TABLE I: Example: Incorporating uncertainty into the behavioral policy considering $\beta = 0.5$. Standard SARSA chooses a_4 , while our algorithm prefers a_2 . The safest available action is a_1 .

Action	$Q(s, a)$	$U(s, a)$	$Q(s, a) - \beta U(s, a)$
a_1	0.2	0.21	0.09
a_2	0.3	0.37	0.112
a_3	0.1	0.78	-0.29
a_4	0.4	0.62	0.087

policy with respect to $Q(s, a)$, and π_t^b as the ϵ -greedy policy with respect to $Q(s, a) - \beta U(s, a)$ as in 13. For each $s \in \mathcal{S}$, define the set of unsafe actions:

$$\mathcal{A}_u(s) = \{a \in \mathcal{A} : \mathcal{T}(s' \in \mathcal{S}_u | s, a) \geq \delta\}$$

where $\mathcal{T}(s' \in \mathcal{S}_u | s, a) = \sum_{s' \in \mathcal{S}_u} \mathcal{T}(s' | s, a)$, and $\delta > 0$ is a threshold. Assume the Markov chains induced by the limiting policies π^0 and $\pi^b = \lim_{t \rightarrow \infty} \pi_t^b$ are irreducible and aperiodic. For sufficiently large β and under the conditions:

- 1) $\sum_t \alpha_t(s, a) = \infty$,
- 2) $\sum_t \alpha_t(s, a)^2 < \infty$,
- 3) $\mathcal{R}(s, a)$ is bounded,

there exists a constant $0 < c < 1$ such that:

$$\lim_{t \rightarrow \infty} \Pr_{\pi_t^b} [s \in \mathcal{S}_u] \leq c \cdot \Pr_{\pi^0} [s \in \mathcal{S}_u]. \quad (14)$$

Proof: Since \mathcal{S} and \mathcal{A} are finite, any stationary policy $\pi : \mathcal{S} \rightarrow \mathcal{P}(\mathcal{A})$ ($\mathcal{P}(\mathcal{A})$ represents the space of probability distributions over \mathcal{A}) induces a Markov chain with transition matrix:

$$P_\pi(s' | s) = \sum_{a \in \mathcal{A}} \pi(a | s) \mathcal{T}(s' | s, a).$$

Given that the Markov chains under π^0 and π^b are irreducible and aperiodic, they each have unique stationary distributions μ_{π^0} and μ_{π^b} , respectively, satisfying:

$$\mu_\pi(s') = \sum_{s \in \mathcal{S}} \mu_\pi(s) P_\pi(s' | s), \quad \sum_{s \in \mathcal{S}} \mu_\pi(s) = 1.$$

The long-run probability of being in \mathcal{S}_u under policy π is:

$$\Pr_\pi [s \in \mathcal{S}_u] = \mu_\pi(\mathcal{S}_u) = \sum_{s \in \mathcal{S}_u} \mu_\pi(s).$$

Under the given convergence conditions $\pi_t^b \rightarrow \pi^b$, hence:

$$\lim_{t \rightarrow \infty} \Pr_{\pi_t^b} [s \in \mathcal{S}_u] = \mu_{\pi^b}(\mathcal{S}_u).$$

Let us define the one-step probability of entering an unsafe state from state s under policy π :

$$p_\pi(s) = \mathcal{T}(s' \in \mathcal{S}_u | s, \pi) = \sum_{a \in \mathcal{A}} \pi(a | s) \mathcal{T}(s' \in \mathcal{S}_u | s, a).$$

For π^0 and π^b , the ϵ -greedy policy is 5 and 13, respectively. We assume that $U(s, a) \geq \eta > 0$ for $a \in \mathcal{A}_u(s)$ and $U(s, a) < \eta$ for $a \notin \mathcal{A}_u(s)$, reflecting that unsafe actions have higher uncertainty. For sufficiently large β , if there exists $a_s \notin \mathcal{A}_u(s)$ with competitive $Q(s, a_s)$, then:

$$Q(s, a_s) - \beta U(s, a_s) > Q(s, a) - \beta U(s, a), \quad \forall a \in \mathcal{A}_u(s)$$

Since $\beta U(s, a) \geq \beta \eta$ is large for unsafe actions, the greedy action under π^b satisfies $a^* = \arg \max_{a'} [Q(s, a') - \beta U(s, a')] \notin \mathcal{A}_u(s)$. Under π^b , if β is large, since $\mathcal{T}(s' \in \mathcal{S}_u | s, a^*) < \delta$, and π^0 selects $a \in \mathcal{A}_u(s)$ with higher probability, typically $p_{\pi^b}(s) < p_{\pi^0}(s)$. Then, we define $A = \mathcal{S}_u$, $B = \mathcal{S} \setminus \mathcal{S}_u$. The flow balance in steady state gives:

$$\sum_{s \in B} \mu_\pi(s) p_\pi(s) = \sum_{s \in A} \mu_\pi(s) [1 - p_\pi(s)].$$

Let $\alpha_\pi = \sum_{s \in B} \mu_\pi(s)p_\pi(s)$, the flow into A . If $p_{\pi^b}(s) < p_{\pi^0}(s)$ for $s \in B$, and assuming $p_{\pi^b}(s) \approx p_{\pi^0}(s)$ for $s \in A$ (similar behavior in unsafe states), then $\alpha_{\pi^b} < \alpha_{\pi^0}$. Suppose there exists $\gamma > 0$ such that $1 - p_\pi(s) \geq \gamma$ for $s \in A$. Then:

$$\mu_\pi(A)[1 - p_\pi(s)]_{\text{avg}} = \alpha_\pi, \quad \mu_\pi(A) \leq \frac{\alpha_\pi}{\gamma}.$$

Therefore, $\mu_{\pi^b}(A) \leq \frac{\alpha_{\pi^b}}{\gamma} < \frac{\alpha_{\pi^0}}{\gamma} \leq \mu_{\pi^0}(A)$. Let us define $c = \frac{\alpha_{\pi^b}}{\alpha_{\pi^0}}$, where $0 < c < 1$. Since $\alpha_{\pi^b} < \alpha_{\pi^0}$, we have:

$$\lim_{t \rightarrow \infty} \Pr_{\pi_t^b}[s \in \mathcal{S}_u] = \mu_{\pi^b}(\mathcal{S}_u) \leq c \cdot \mu_{\pi^0}(\mathcal{S}_u) = c \cdot \Pr_{\pi^0}[s \in \mathcal{S}_u]$$

and the proof is complete. \blacksquare

IV. EXPERIMENTS

We evaluate OT-guided SARSA in three case studies with different sources of environment uncertainty, which can influence the decision-making process. In particular, we focus on stochastic reward function, stochastic transition dynamics, and stochastic observation function (Fig. 3). For all case studies, the cost matrix used for computing the uncertainty score is $C_{ij} = 1$ if $i \neq j$, and 0 otherwise. Furthermore, $\gamma = 0.99$ and $\epsilon = 0.1$ for all case studies.

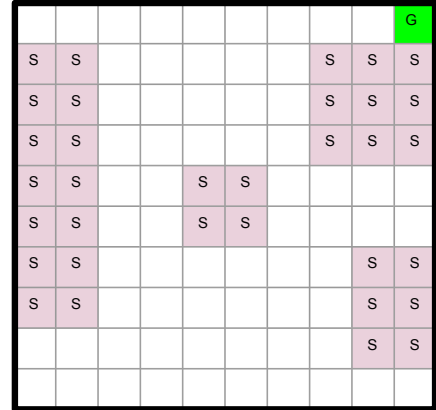
A. CASE STUDY 1: GRID-WORLD WITH REWARD UNCERTAINTY

We consider a 10×10 grid-world environment with normal, goal, and slippery states [15]. The agent can move up, down, left, and right. For any movement to a normal state, the agent receives the reward of -1 , while transitions to slippery states result in a random reward in the range $[-12, 10]$. Collisions with walls incur a reward of -10 . The episode terminates when the agent either reaches the goal state in the top-right corner or completes a maximum of 100 steps.

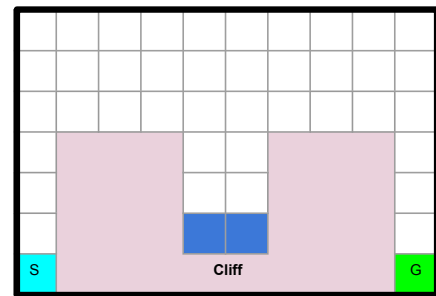
The results in Fig. 4 demonstrate that the OT-guided SARSA algorithm converges to a higher return value and exhibits higher stability throughout the learning process, mainly because of the uncertainty score term, which guides exploration toward safer and more consistent actions. Furthermore, we present the state visitation map in Fig. 5. As expected, SARSA algorithm demonstrates a high frequency of visits to slippery regions (darker red). In contrast, Q-learning performs better by exploring more efficient paths, but it still exhibits notable visits to unsafe states in comparison to our algorithm.

B. CASE STUDY 2: CLIFF WALKING WITH TRANSITION UNCERTAINTY

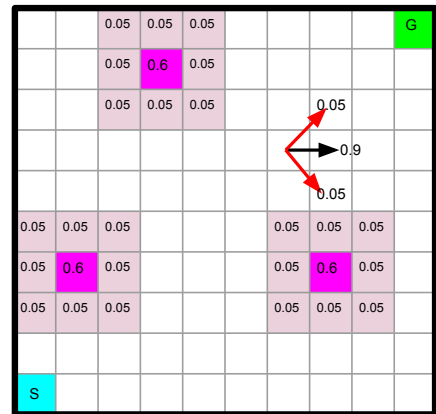
This environment consists of three zones: the cliff, the trap, and the feasible regions. The agent starts at the bottom-left corner to reach the goal at the bottom-right corner while avoiding the cliff region [39]. The agent can move freely within the feasible region in four directions: up, down, left, and right. Entering the cliff region results in task failure. Entering the trap region forces the agent to move downward, regardless of its chosen action, eventually ending up in the cliff region. Each movement yields a reward of -1 . If the



(a) Grid-world environment



(b) Cliff walking case study



(c) Rover navigation task

Fig. 3: Case studies: Grid-world featuring reward uncertainty, Cliff walking with traps featuring transition function uncertainty, Rover navigation task involving partial observability in obstacle locations.

agent collides with the environment borders, its position remains unchanged, but it still earns the movement reward. Reaching the target earns the agent a reward of 101, while entering the cliff region results in a -49 penalty. Upon reaching either the target or the cliff region, the training

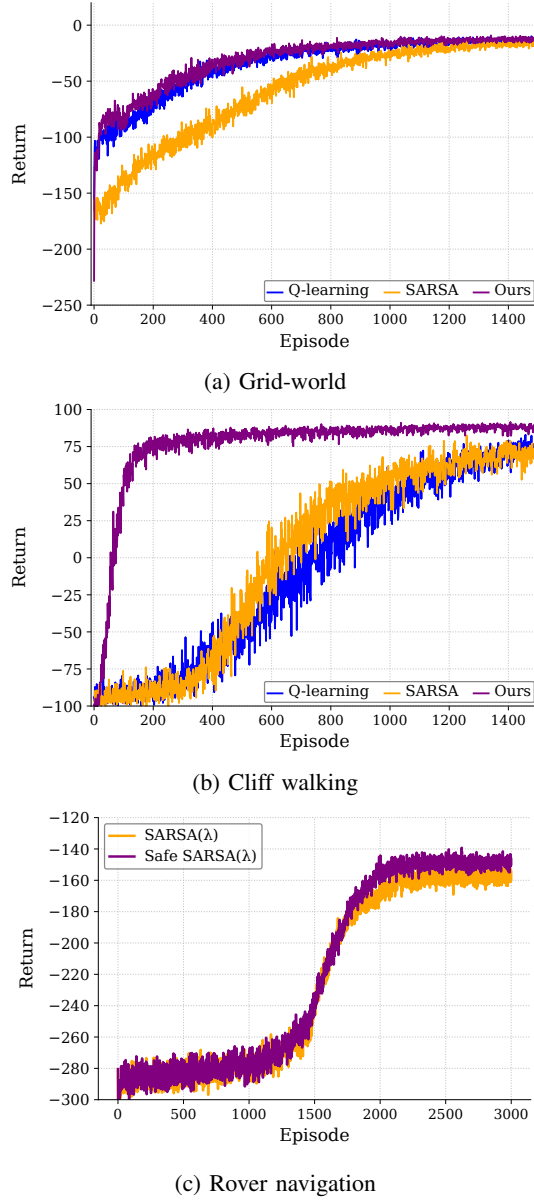


Fig. 4: Comparison between average cumulative reward over 50 random seeds. In all case studies, our algorithm outperforms other baselines.

episode restarts, and the agent is reset to its starting position.

As shown in Fig. 4 for this case study, our algorithm achieves rapid convergence, mainly because of prioritizing less uncertain actions. It also demonstrates a higher confidence in its return estimates. In contrast, both Q-learning and SARSA display greater variability, which reflects higher uncertainty in their returns. For this case study, the state visitation graph in Fig. 8 highlights the limitations of SARSA, where the agent struggles to identify the optimal path to the goal state. Consequently, most episodes end without successfully reaching the goal. Q-learning performance is closer to our algorithm, however, the rate of reaching the goal and escaping from the cliff in the initial episodes is lower than ours.

C. CASE STUDY 3: ROVER NAVIGATION WITH PARTIAL OBSERVABILITY

In this case study, a rover must navigate a two-dimensional terrain map represented as a 10×10 grid, where 3 of the grid cells are obstacles [40]. Each grid cell represents a state, and the rover can move in eight geographic directions. However, the environment is stochastic; for example, as shown in Fig. 3, when the rover takes the action east, it moves to the intended grid cell with a probability of 0.9 but may move to one of the adjacent cells with a probability of 0.05. Partial observability exists because the rover cannot directly detect the locations of obstacle cells through its measurements. When the rover moves to a cell adjacent to an obstacle, it can identify the exact location of the obstacle (magenta) with a probability of 0.6 and observe a probability distribution over nearby cells (pink). Colliding with an obstacle results in an immediate penalty of 10, while reaching the goal region provides no immediate reward. All other grid cells impose a penalty of 2.

As demonstrated in Fig. 4, OT-guided SARSA(λ) achieves superior performance compared to standard SARSA(λ).

D. ABLATION STUDY

Performance under varying uncertainty and scale: We further analyze the performance of our algorithm under different levels of uncertainty and environment size. In particular, we consider the above settings as low uncertainty (LU). To model high uncertainty (HU) in the grid-world scenario, we increase the number of slippery states from 33 to 50, while for cliff walking, we enhance the number of traps from 2 to 6 to have more stochasticity in the environment. For the POMDP case study, we raised the number of partially observable obstacles from 3 to 10 to amplify the level of uncertainty. Additionally, to assess the impact of environment size on agent performance, we expand the grid-world and rover navigation tasks from 10×10 to 30×30 , and the cliff walking from 7×10 to 21×30 .

Table. II, III, and IV present a quantitative comparison of OT-guided SARSA performance to other baselines, providing the average return and standard deviation (std) under LU, HU, and increasing environment size scenarios across last 20 episodes for all case studies. The results in the Table. II, and III confirm that OT-guided SARSA achieves the highest return and the lowest std in different scenarios. Moreover, in the cliff walking case study, the number of failures for our agent is significantly lower than both SARSA and Q-learning. For instance, in the LU scenario, OT-guided SARSA reduces failures by 35% compared to SARSA and 30% compared to Q-learning. This reduction is even greater in the other two scenarios. Overall, in both MDP case studies, our algorithm obtained a higher cumulative reward than Q-learning and SARSA, while improving the stability and the safety of the agent by avoiding unpredictable actions. Furthermore, for both MDP case studies, although increasing the size of the environment causes lower return values, OT-guided SARSA still maintains the best performance.

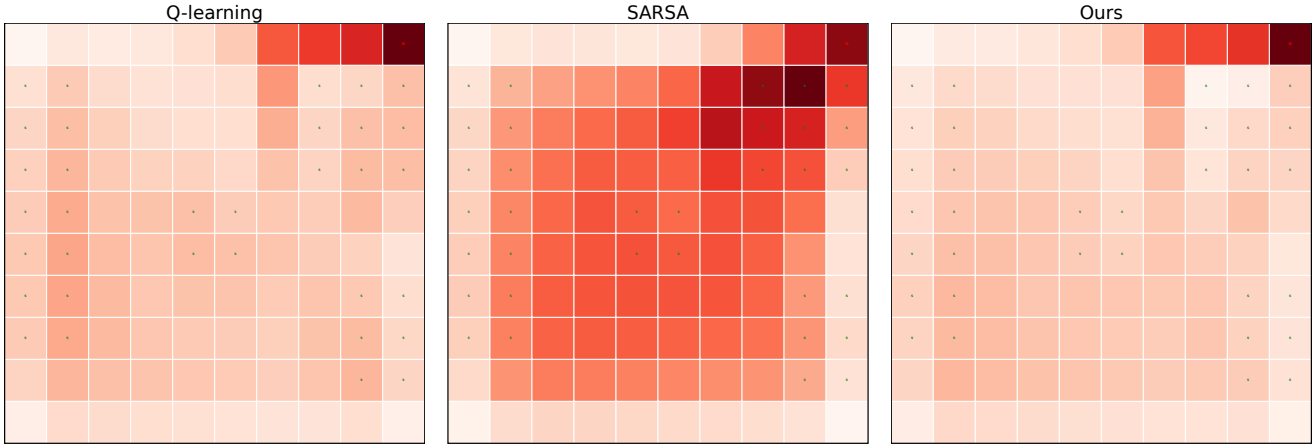


Fig. 5: Comparison between state visitation density on grid-world case study. Our algorithm visitation to slippery states with reward uncertainty is less than both SARSA and Q-learning.

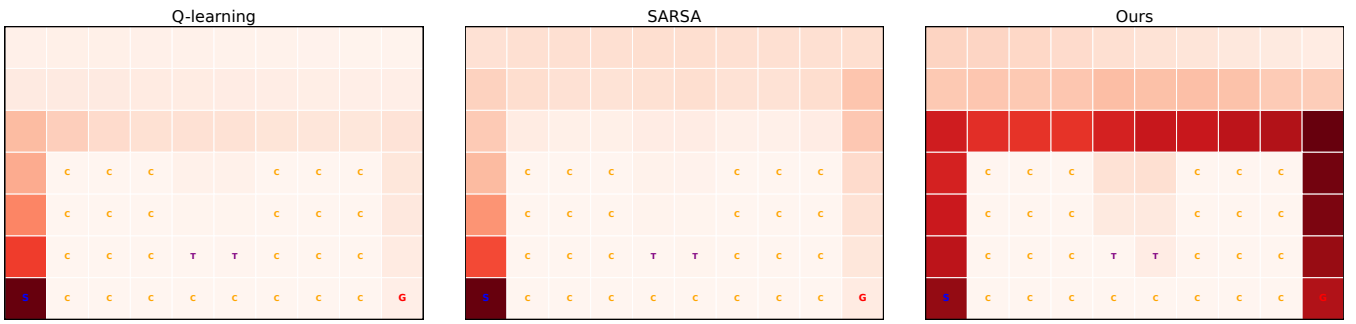


Fig. 6: Comparison between the density of state visitation on the cliff walking case study. Our algorithm provides fewer visits to the cliff region than SARSA and Q-learning, and reaches the goal state more often (darker red).

TABLE II: Ablation study on grid-world environment. Average return and std over different algorithms for low-uncertainty (LU), high-uncertainty (HU), and large state space scenarios.

Scenario	SARSA	Q-learning	Ours
10 × 10 LU	-15.70 ± 17.32	-13.38 ± 14.53	-12.04 ± 12.83
10 × 10 HU	-16.26 ± 20.38	-14.14 ± 18.52	-12.92 ± 16.79
30 × 30 HU	-119.16 ± 126.65	-108.21 ± 118.76	-98.77 ± 112.15

TABLE III: Ablation study on cliff walking case study. Average performance metrics for low-uncertainty (LU), high-uncertainty (HU), and large state space scenarios.

Scenario	Return/Failures	SARSA	Q-learning	Ours
10 × 7 LU	return \pm std	72.48 ± 36.1	74.59 ± 28.52	87.99 ± 10.65
	failures	72.74	61.46	21.74
10 × 7 HU	return \pm std	69.82 ± 38.69	84.27 ± 23.99	89.53 ± 8.65
	failures	196.94	77.56	30.14
30 × 21 HU	return \pm std	-177.07 ± 54.61	42.11 ± 37.44	55.59 ± 22.36
	failures	523.64	362.66	196.48

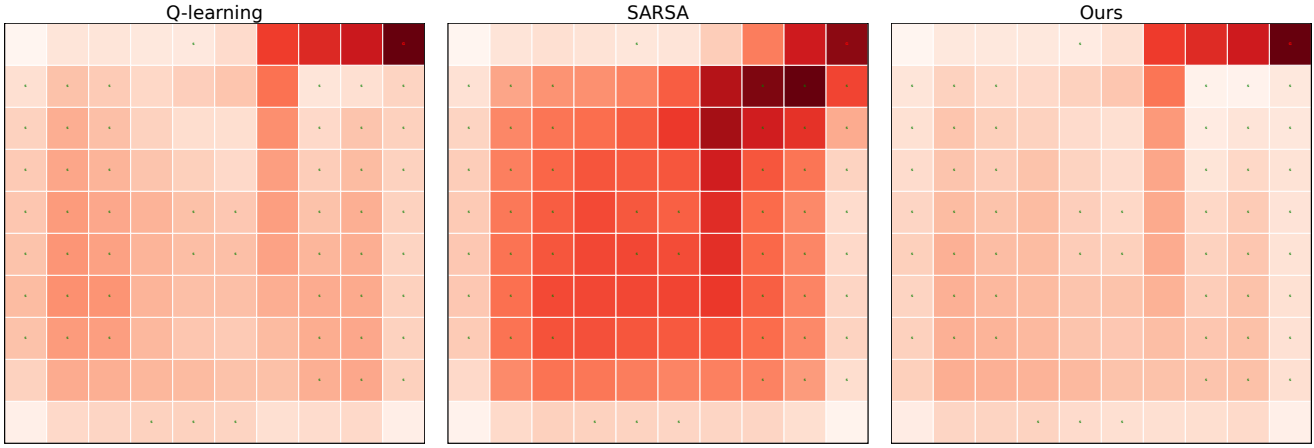


Fig. 7: Comparison between state visitation density for different algorithms on grid-world with high uncertainty. Our algorithm visits slippery states less frequently than both baselines.

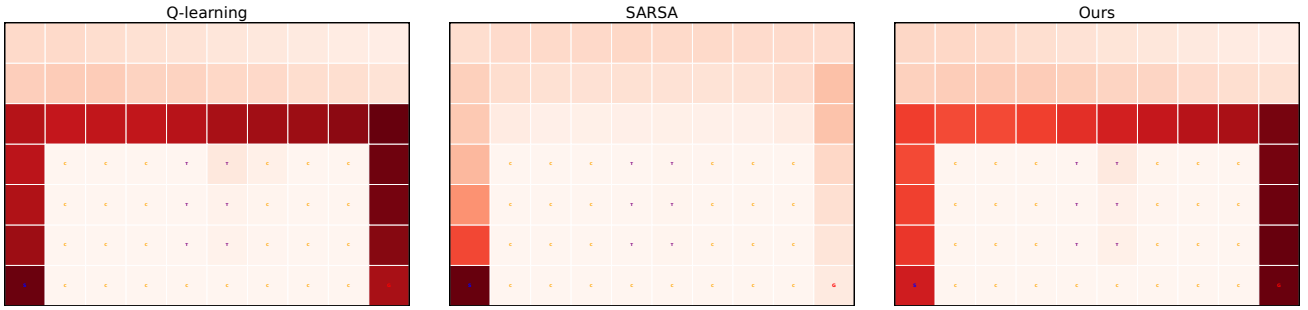


Fig. 8: Comparison between the density of state visitation for different algorithms in the case of cliff walking with high uncertainty. While both our algorithm and Q-learning agents were able to find the optimal path to the goal state, our algorithm fell to the cliff states less often.

TABLE IV: Ablation study on rover navigation task. Average performance metrics for low-uncertainty (LU), high-uncertainty (HU), and large state space scenarios.

Scenario	Return/Failures	SARSA(λ)	Ours
10 \times 10 LU	return \pm std	-155.04 ± 109.09	-149.96 ± 106.41
	failures	2805.73	2663.48
10 \times 10 HU	return \pm std	-247.70 ± 102.58	-264.00 ± 89.72
	failures	9039.29	8948.18
30 \times 30 HU	return \pm std	-1024.74 ± 57.09	-1020.70 ± 39.26
	failures	30725.38	30026.71

For the POMDP case study, as can be seen in the Table. IV, by increasing the partial observability degree (HU), the agent performance falls back. This shows that the performance of our algorithm can be influenced by the degree of partial observability in the environment. Specifically, when the agent receives indistinguishable or highly similar observations for different underlying states, the accuracy of the estimated Q-values, target distribution, and, consequently, the reliability

of the uncertainty score becomes questionable. The number of failures for OT-guided SARSA(λ) across the three scenarios is slightly lower than SARSA(λ).

Sensitivity analysis of safety coefficient β : We additionally provide a sensitivity analysis on the hyperparameter β . Fig. 9 depicts the learning curve for different β values for the cliff walking case study. As β increases, the agent prioritizes safety more strongly, which reduces its willingness to explore

potentially risky but rewarding paths. When β is small, the uncertainty score has less impact on Q-values, which causes the algorithm to behave similarly to standard SARSA. This trade-off highlights the importance of carefully tuning β to achieve an appropriate balance between safety and performance.

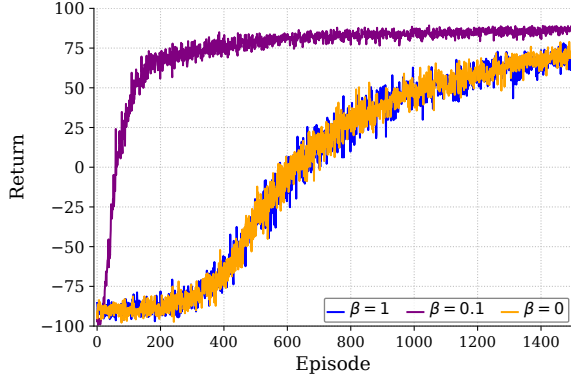


Fig. 9: Sensitivity analysis of hyperparameter β in cliff walking case study.

V. CONCLUSION

We presented an uncertainty-oriented TD algorithm based on optimal transport theory. We showed the effectiveness of this approach in encouraging agent to prioritize less uncertain actions, leading to a reduction in visits to unsafe states and an improvement in cumulative rewards. Compared to standard TD algorithms, our algorithm demonstrated robust performance in environments with reward, transition, and state uncertainties. Although our algorithm outperforms standard TD learning methods, it has its limitations. Determining the optimal transport map for candidate actions at each state is computationally expensive. While using the entropy-regularized extension of OT reduces this computational cost, further improvements in computational efficiency will be a focus of future work. Another future direction is the extension of our algorithm to constrained MDPs in which the agent seeks to maximize the expected return while satisfying some constraints, typically expressed as bounds on expected costs. The optimal transport formulation could then be adapted by modifying its cost matrix to reflect these constraints. Finally, investigating our algorithm in the continuous domain by considering the distribution of action preferences derived from Q-values approximated as Gaussian is feasible and cost-efficient because Wasserstein distance provides a closed-form solution for Gaussian distributions. This would be an interesting direction to facilitate the integration of our approach into robotic control and autonomous navigation applications.

REFERENCES

- [1] F. Richter, R. K. Orosco, and M. C. Yip, “Open-sourced reinforcement learning environments for surgical robotics,” *arXiv preprint arXiv:1903.02090*, 2019.
- [2] A. Kendall, J. Hawke, D. Janz, P. Mazur, D. Reda, J.-M. Allen, V.-D. Lam, A. Bewley, and A. Shah, “Learning to drive in a day,” in *International Conference on Robotics and Automation (ICRA)*, IEEE, 2019, pp. 8248–8254.
- [3] B. Hambly, R. Xu, and H. Yang, “Recent advances in reinforcement learning in finance,” *Mathematical Finance*, vol. 33, no. 3, pp. 437–503, 2023.
- [4] S. Gu, L. Yang, Y. Du, G. Chen, F. Walter, J. Wang, and A. Knoll, “A review of safe reinforcement learning: Methods, theories and applications,” *IEEE Transactions on Pattern Analysis and Machine Intelligence*, 2024.
- [5] J. Garcia and F. Fernández, “A comprehensive survey on safe reinforcement learning,” *Journal of Machine Learning Research*, vol. 16, no. 1, pp. 1437–1480, 2015.
- [6] M. Heger, “Consideration of risk in reinforcement learning,” in *Machine Learning Proceedings*, Elsevier, 1994, pp. 105–111.
- [7] C. Gaskett, “Reinforcement learning under circumstances beyond its control,” *International Conference on Computational Intelligence for Modelling Control and Automation*, 2003.
- [8] M. Sato, H. Kimura, and S. Kobayashi, “TD algorithm for the variance of return and mean-variance reinforcement learning,” *Transactions of the Japanese Society for Artificial Intelligence*, vol. 16, no. 3, pp. 353–362, 2001.
- [9] P. Geibel and F. Wysotski, “Risk-sensitive reinforcement learning applied to control under constraints,” *Journal of Artificial Intelligence Research*, vol. 24, pp. 81–108, 2005.
- [10] J. Achiam, D. Held, A. Tamar, and P. Abbeel, “Constrained policy optimization,” in *International Conference on Machine Learning*, PMLR, 2017, pp. 22–31.
- [11] Y. Chow, O. Nachum, A. Faust, E. Duenez-Guzman, and M. Ghavamzadeh, “Lyapunov-based safe policy optimization for continuous control,” *arXiv preprint arXiv:1901.10031*, 2019.
- [12] L. Brunke, M. Greeff, A. W. Hall, Z. Yuan, S. Zhou, J. Panerati, and A. P. Schoellig, “Safe learning in robotics: From learning-based control to safe reinforcement learning,” *Annual Review of Control, Robotics, and Autonomous Systems*, vol. 5, no. 1, pp. 411–444, 2022.
- [13] Y. Okawa, T. Sasaki, H. Yanami, and T. Namerikawa, “Safe exploration method for reinforcement learning under existence of disturbance,” in *Joint European Conference on Machine Learning and Knowledge Discovery in Databases*, Springer, 2022, pp. 132–147.
- [14] J. Dai, X. Pan, R. Sun, J. Ji, X. Xu, M. Liu, Y. Wang, and Y. Yang, “Safe RLHF: Safe reinforcement learning from human feedback,” *arXiv preprint arXiv:2310.12773*, 2023.
- [15] C. Gehring and D. Precup, “Smart exploration in reinforcement learning using absolute temporal difference errors,” in *International Conference on Autonomous Agents and Multi-agent Systems*, 2013, pp. 1037–1044.
- [16] E. L. Law, “Risk-directed exploration in reinforcement learning,” *PhD thesis*, 2005.
- [17] B. O’Donoghue, I. Osband, R. Munos, and V. Mnih, “The uncertainty Bellman equation and exploration,” in *International Conference on Machine Learning*, 2018, pp. 3836–3845.
- [18] P. Malekzadeh, M. Hou, and K. N. Plataniotis, “A unified uncertainty-aware exploration: Combining epistemic and aleatory uncertainty,” in *IEEE International Conference on Acoustics, Speech and Signal Processing (ICASSP)*, 2023, pp. 1–5.
- [19] W. Dabney, M. Rowland, M. Bellemare, and R. Munos, “Distributional reinforcement learning with quantile regression,” in *Proceedings of the AAAI conference on Artificial Intelligence*, vol. 32, 2018.
- [20] B. Mavrin, H. Yao, L. Kong, K. Wu, and Y. Yu, “Distributional reinforcement learning for efficient exploration,” in *International Conference on Machine Learning*, PMLR, 2019, pp. 4424–4434.
- [21] F. Zhou, Z. Zhu, Q. Kuang, and L. Zhang, “Non-decreasing quantile function network with efficient exploration for distributional reinforcement learning,” *arXiv preprint arXiv:2105.06696*, 2021.
- [22] Y. Tang and S. Agrawal, “Exploration by distributional reinforcement learning,” *arXiv preprint arXiv:1805.01907*, 2018.
- [23] M. Chen, X. Xiao, W. Zhang, and X. Gao, “Efficient and stable information directed exploration for continuous reinforcement learning,” in *IEEE International Conference on Acoustics, Speech and Signal Processing (ICASSP)*, 2022, pp. 4023–4027.

- [24] N. Nikolov, J. Kirschner, F. Berkenkamp, and A. Krause, “Information-directed exploration for deep reinforcement learning,” *arXiv preprint arXiv:1812.07544*, 2018.
- [25] T. Yu, G. Thomas, L. Yu, S. Ermon, J. Y. Zou, S. Levine, C. Finn, and T. Ma, “MOPO: Model-based offline policy optimization,” *Advances in Neural Information Processing Systems*, vol. 33, pp. 14 129–14 142, 2020.
- [26] F. Santambrogio, *Optimal transport for applied mathematicians*. Springer, 2015, vol. 87.
- [27] A. Baheri, “Risk-aware reinforcement learning through optimal transport theory,” *arXiv preprint arXiv:2309.06239*, 2023.
- [28] A. Baheri, “Understanding reward ambiguity through optimal transport theory in inverse reinforcement learning,” in *NeurIPS Workshop Optimal Transport and Machine Learning*, 2023.
- [29] J. Queeney, E. C. Ozcan, I. C. Paschalidis, and C. G. Cassandras, “Optimal transport perturbations for safe reinforcement learning with robustness guarantees,” *arXiv preprint arXiv:2301.13375*, 2023.
- [30] A. M. Metelli, A. Likmeta, and M. Restelli, “Propagating uncertainty in reinforcement learning via Wasserstein barycenters,” *Advances in Neural Information Processing Systems*, vol. 32, 2019.
- [31] Z. Shahrooei and A. Baheri, “Optimal transport-assisted risk-sensitive Q-learning,” *arXiv preprint arXiv:2406.11774*, 2024.
- [32] A. Baheri, Z. Shahrooei, and C. Salgarkar, “Wasserstein adaptive value estimation for actor-critic reinforcement learning,” *arXiv preprint arXiv:2501.10605*, 2025.
- [33] R. M. Nkhumise, D. Basu, T. J. Prescott, and A. Gilra, “Studying exploration in RL: An optimal transport analysis of occupancy measure trajectories,” *Transactions on Machine Learning Research*, 2025, ISSN: 2835-8856.
- [34] R. S. Sutton and A. G. Barto, *Reinforcement learning: An introduction*. MIT press Cambridge, 1998, vol. 1.
- [35] C. J. Watkins and P. Dayan, “Q-learning,” *Machine Learning*, vol. 8, pp. 279–292, 1992.
- [36] V. Krishnamurthy, *Partially observed Markov decision processes*. Cambridge University Press, 2016.
- [37] C. Villani, *Optimal transport: old and new*. Springer, 2009, vol. 338.
- [38] M. Cuturi, “Sinkhorn distances: Lightspeed computation of optimal transport,” *Advances in Neural Information Processing Systems*, vol. 26, 2013.
- [39] C. Xuan, F. Zhang, and H.-K. Lam, “SEM: Safe exploration mask for Q-learning,” *Engineering Applications of Artificial Intelligence*, vol. 111, p. 104 765, 2022.
- [40] M. Ahmadi, U. Rosolia, M. D. Ingham, R. M. Murray, and A. D. Ames, “Risk-averse decision making under uncertainty,” *IEEE Transactions on Automatic Control*, vol. 69, no. 1, pp. 55–68, 2023.